Bassey et al.
Journal of Engineering and Applied Science (2024) 71:33
https://doi.org/10.1186/s44147-024-00375-0

Journal of Engineering and Applied Science

RESEARCH Open Access

# Thermal analysis of AISI 1020 low carbon steel plate agglutinated by gas tungsten arc welding technique: a computational study of weld dilution using finite element method

Michael Okon Bassey[1*], Jephtar Uviefovwe Ohwoekevwo[2] and Aniekan Essienubong Ikpe[3]

*Correspondence: michaelobassey@gmail.com

[1] Department of Mechatronics Engineering, Akwa Ibom State Polytechnic, Ikot Ekpene PMB 1200, Nigeria
[2] Department of Production Engineering, University of Benin, Benin City PMB 1154, Nigeria
[3] Department of Mechanical Engineering, Akwa Ibom State Polytechnic, Ikot Ekpene PMB 1200, Nigeria

## Abstract

An important goal in a number of optimization studies is a high-quality weld joint. Thermal analysis of AISI 1020 low carbon steel plate agglutinated by gas tungsten arc welding technique was carried out using S 2021 version. With SOLIDWORKS Premium, the simulation was run. The simulation was performed using the Thermal Simulation programme with 20 weld runs. With the findings of the initial study serving as a sensor, a design study was conducted. A total of 15 runs were completed, and the weld dilution and thermal conductivity responses were available. A range of welding temperatures including 3397 to 3688 °C were experimentally applied in the joining process of AISI 1020 low carbon steel plate of 10 mm thickness, and a strain gauge indicator was used to measure the thermal stresses induced in the steel plate. However, minimum and maximum weld dilution values of 73.1 and 46.8% were obtained with FEM at an input of arc heat of 66.4 and 37.2 J/mm, while the minimum and maximum weld dilution values of 71.55 and 45.5% were computed using experimental approach at the same heat input. On the other hand, maximum and minimum weld dilution of 71.55 and 44.5% were computed from experimental process at minimum and maximum welding current of 199.77 and 250.23 A, while 73.1 and 46.8% were obtained for the maximum and minimum weld dilution through FEM procedure at the same welding input variables. Hence, gas tungsten arc welding input parameters should be properly selected and controlled during welding operation, in order to minimize thermal effects and welding flaws such as high dilution rate.

**Keywords:** TIG welding, Finite element analysis, Weld dilution, Mild steel, Welding current

## Introduction

Gas tungsten arc welding (GTAW) otherwise known as tungsten inert gas (TIG) is a process that involves fusion of two or more materials together through the localized application of heat, which results in melting and dilution of the weld (fusion zone). This results in alteration of the chemical and mechanical properties, which upon cooling is characterized by the chemical composition of the bead and filler material. The area surrounding the fusion line is known as heat-affected zone (HAZ), an area that is partially heated completely but not withstanding which has been affected by the welding thermal and thermo-elasto-plastic cycle [1, 2].

The direct consequence of dilution is the difference in chemical composition of the final weld metal from both the base and filler materials, producing a new deposit alloy intermediate between the two. The change in chemical composition resulting from dilution will affect the phase transformation kinetics during weld-induced thermal cycles, as well as the resultant microstructures [3]. The effects of weld dilution on the microstructural and mechanical properties of a steel weld can be significant even when the chemical mismatch is marginal [4, 5].

Hunt et al. [6] considered bead-on-plate submerged arc (SA) welding in micro-alloyed steel and observed that low-dilution welds had inclusions of a larger mean size in comparison with high-dilution welds. It was observed that the weld exhibited higher fractions of finer acicular ferrite and superior toughness. However, for multi-pass welding, dilution effects were exacerbated by thermal cycling.

Sehrawat [7] developed a mathematical model to predict weld dilution in gas metal arc welding (GMAW) of stainless steel 301 using response surface methodology (RSM). A total of 28.24% was obtained as the minimum value of dilution (from weld run no. 27), while a maximum value of 70.27% was obtained as weld dilution (from weld run no. 30). Nozzle-to-plate distance (NPD), welding torch angle, and welding voltage had a negative effect on weld dilution, whereas wire feed rate (WFR) had a positive effect and welding speed having negligible effect on weld dilution. However, Lu et al. [8] reported that by increasing the wire feeding speed under the condition of pulse peak current and reducing the welding speed, a high deposition efficiency, low dilution rate, and low heat input may be obtained.

Aghakhani et al. [9] employed the fuzzy logic technique to investigate the effects of wire feed rate, arc voltage, nozzle-to-plate distance, welding speed, and gas flow rate on weld dilution using gas metal arc welding (GMAW) process. Weld dilution was observed to increase with an increase in wire feed rate and arc voltage as a result of an increase in welding heat input. Moreover, weld dilution was also observed to decrease with an increase in nozzle-to-plate distance and welding speed as a result of a decrease in welding heat input. In addition, an increase in gas flow rate initially increased weld dilution, but eventually, further increase in gas flow rate led to a decrease in weld dilution.

Sun et al. [10] determined weld dilution for each bead in a three-pass gas tungsten arc (GTA) weld and a corresponding submerged arc (SA) weld. Different filler materials were used with each process, but both cases involved the deposition of filler wires into grooves in low-alloy (SA508) ferritic steel plates. The modelling revealed that increases in weld dilution favour the formation of martensite but suppress bainite/ferrite transformations, due to the melting of greater quantities of the base material, which had a relatively high hardenability.

Sun et al. [11] investigated the effects of dilution on the hardness and residual stresses in multi-pass steel welds. For the base and filler materials used, increased dilution led to greater weld-metal hardness and reduced the magnitude of tensile stress or promoted compressive stress in the as-deposited and reheated weld metals. This mechanical behaviour is associated with the tendency for diluted weld metal to experience delayed austenite decomposition, due to the high hardenability of the SA508 steel relative to the filler materials used.

Zhang et al. [12] proposed a new method for weld dilution calculation using chemical composition analysis. It was observed that whether a certain composition is diluted or concentrated, an increase in the welding heat input causes the compositions' concentration to be at the same level as the original substrate. However, the dilution becomes stable once the heat input exceeds a transition point of 0.18 kJ/mm which may result from adequate convection of the molten pool due to high-level heat input. In other words, the weld dilution value changes rapidly before the heat input attains a transition point of 0.18 kJ/mm, while the weld dilution stabilizes once the heat input is beyond the transition point. This paper involved the computational study of weld dilution using the finite element method to validate thermal analysis of AISI 1020 low carbon steel plate agglutinated experimentally via gas tungsten arc welding technique. In this study, experimental and FEM weld dilution at different heat input, experimental and FEM weld dilution at different melting rates, experimental and FEM weld dilution at multiple weld parameters, and experimental and FEM weld dilution at different welding currents were determined. Weld dilution simulation profiles at different welding intervals and maximum welding temperatures were also determined.

## Methods

Low carbon steel plate AISI 1020 with a 10 mm thickness was cut into dimensions of $60 \times 40 \times 10$ mm (long × breadth × width). Before welding the samples, rough particles and rust were removed from the surface of the specimen using emery paper (coarse: P24 grit size with 715 m and fine: P80 grit size with 201 m).

The surface of the samples to be welded was then cleaned with acetone to remove any surface contaminants. The welding sample (plate) was clamped to a G-clamp and chamfered (2 mm depth) with 45° at the edge to create a V-groove angle using a vertical milling machine. A vertical milling machine was used to provide the milling angle. To prevent misalignment during the welding process, the plates were securely secured during welding. The plate's chamfered area was subjected to TIG welding, with a 2% thoriated tungsten electrode used to fill the chamfered area.

This was accomplished by using a Dynasty 210 DX welding machine and 100% argon torch gas to keep the welding area clean. A recent work on the use of SEM/EDS in a fractographic investigation of TIG-welded AISI 1020 fusion zones at different welding current steps by Owunna et al. [13] used a similar methodology. Table 1 presents the TIG welding requirements that were used during the welding procedure, and Fig. 1 displays samples of the steel plates that were welded.

The welding temperature was measured at several spots along the workpiece's surface using K-type thermocouples as the arc travelled through it. Additionally, the welding torch moved over the plate at a constant speed of 1.72 m/s while being 2.5 mm away from the workpiece. To prevent any systematic inaccuracy in the experiment, the welding trials were conducted in accordance with the central composite design matrix (CCD) in Table 2 and in a random order. Figure 1 displays the welded samples.

To create test specimens, the welded plates were cross-examined at their axial midpoints after being evaluated for any apparent flaws and homogeneity. Following the

**Table 1** Materials and specifications used for the welding experimentation

| S/no | Material specification | Welding specification |
|---|---|---|
| 1 | Welding type | Tungsten inert gas (TIG) |
| 2 | Material | AISI 1020 low carbon steel plate |
| 7 | Material thickness | 10 mm |
| 8 | Filler material | ER 70 S-6 |
| 9 | Joint type | Butt joint (V-groove) |
| 10 | Joint preparation | Abrasive clean (sandpaper)/acetone wipe |
| 11 | Joint gap | 2 mm |
| 12 | Welding current | DCEN (direct current electrode negative) |
| 13 | Pulse width | 0.8 s |
| 14 | Filler rod angle | 15° |
| 15 | Welding torch angle | 45° |
| 16 | Fixed frequency | 60 Hz |
| 17 | Torch type | Pro-torch (TIG torch) |
| 18 | Tungsten type | 2% thoriated |
| 19 | Tungsten size | 3/1326″ diameter × 25.4 mm |
| 20 | Torch gas | Argon (100%) |
| 21 | Heat input ratio | 10.75 kJ/min |
| 22 | Weight of filler rod | 78.5 kg/m$^2$ |
| 23 | Welding machine | Dynasty 210 DX |
| 24 | Clamp type | G-clamp for clamping the workpiece |
| 25 | Vertical milling machine | For milling the V-groove angle |

Batch A Batch B

**Fig. 1** Mild steel welded samples

completion of all trials, samples were prepared for the measurement of weld dilution by cutting, polishing, and etching these $60 \times 40 \times 10$ mm dimensioned test pieces. As illustrated in Fig. 2, the samples were scanned using an optical microscope at 1:1 scale on a scanner to determine the dilution. Utilizing the same Foxit reader software that was used to calculate the weld dilution by measuring penetration, the bead geometry of these samples was determined.

### Finite element method

The following procedure outlines a systematic approach that was adopted for modelling weld dilution in this study using finite element (FE) method.

i. Material characterization: Accurate material characterization is essential for reliable FE simulations. This step involved obtaining material properties, such as ther-

**Table 2** Central composite design matrix (CCD)

| Std | Weld runs | Block | Current | Voltage | Gas flow rate |
|---|---|---|---|---|---|
| 12 | 1 | Block 1 | 250.23 | 23.5 | 13.5 |
| 16 | 2 | Block 1 | 225 | 26 | 14.5 |
| 10 | 3 | Block 1 | 250.23 | 24.5 | 14.5 |
| 19 | 4 | Block 1 | 240 | 25 | 16 |
| 6 | 5 | Block 1 | 225 | 25 | 16 |
| 13 | 6 | Block 1 | 240 | 20.98 | 13.5 |
| 9 | 7 | Block 1 | 199.77 | 24.5 | 13.5 |
| 18 | 8 | Block 1 | 210 | 25 | 16 |
| 15 | 9 | Block 1 | 199.77 | 26 | 11.98 |
| 14 | 10 | Block 1 | 250.23 | 20.98 | 13.5 |
| 3 | 11 | Block 1 | 240 | 22 | 11.98 |
| 11 | 12 | Block 1 | 225 | 24.5 | 11.98 |
| 5 | 13 | Block 1 | 210 | 22 | 16 |
| 7 | 14 | Block 1 | 199.77 | 23.5 | 14.5 |
| 20 | 15 | Block 1 | 210 | 20.98 | 14.5 |
| 8 | 16 | Block 1 | 225 | 22 | 13.5 |
| 2 | 17 | Block 1 | 199.77 | 26 | 11.98 |
| 17 | 18 | Block 1 | 240 | 20.98 | 13 |
| 4 | 19 | Block 1 | 210 | 22 | 16 |
| 1 | 20 | Block 1 | 250.23 | 22 | 11.98 |

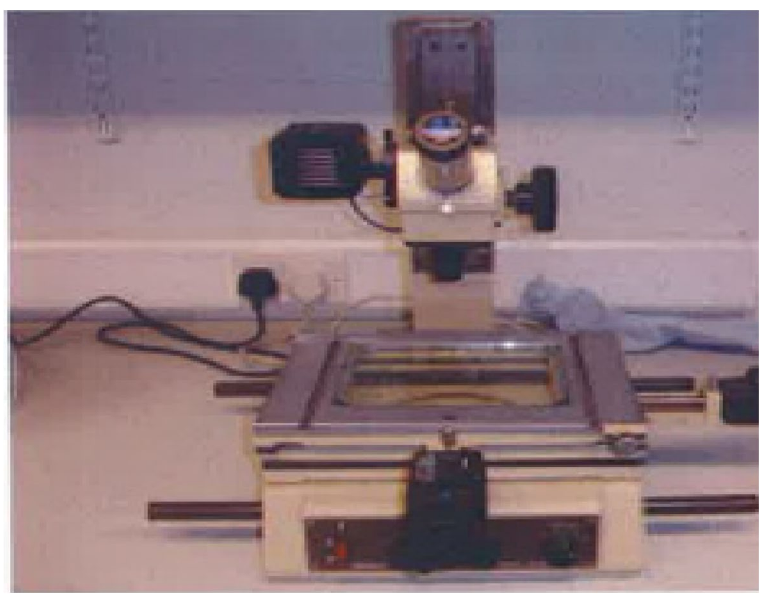

**Fig. 2** Optical microscope

mal conductivity, specific heat, and mechanical properties, through experimental testing. The material properties were then incorporated into the FE model.

ii. Geometry and mesh generation: The geometry of the welded joint was created using computer-aided design (CAD) software known as SOLIDWORKS. The model was divided into finite elements, and a suitable mesh was generated. The mesh density was determined based on the complexity of the geometry and the desired level of accuracy.

iii. Boundary conditions and welding parameters: Boundary conditions, including temperature and displacement constraints, were defined to simulate the welding process accurately. Welding parameters, such as heat input, welding speed, and electrode diameter, were also specified. These parameters significantly influenced the extent of weld dilution.
iv. Heat transfer and fluid flow analysis: The FE model was subjected to heat transfer and fluid flow analysis to simulate the welding process. The heat source model, which represents the welding arc, was incorporated into the simulation. The temperature distribution and fluid flow patterns were obtained, allowing for the prediction of weld dilution.
v. Material mixing and dilution calculation: Based on the temperature distribution and fluid flow patterns, the mixing of base metal and filler material was simulated. The dilution ratio, defined as the percentage of filler material in the weld, was calculated.
vi. Validation and sensitivity analysis: The FE model was validated by comparing the predicted dilution ratio with experimental data. Sensitivity analysis was performed to assess the influence of different welding parameters on weld dilution. This step helped identify critical factors affecting dilution and provided insights for process optimization.

By accurately simulating the welding process and predicting the dilution ratio, welding parameters such as weld dilution at different heat input, weld dilution at different melting rates, weld dilution at multiple weld parameters, and weld dilution at different welding currents were determined. The following highlights were also considered while implementing the systematic approaches adopted for the finite element modelling.

i. Dividing the continuum into a finite number of elements made up of line segments, triangles, quadrilaterals, squares, rectangles, etc.
ii. Choosing important locations on the elements to act as nodes for the application of equilibrium and compatibility requirements
iii. Making the assumption that each individual element's displacement functions depend on the nodal values in order to determine the displacements at each generic point.
iv. Determine the stiffness and equivalent nodal loads for a particular element using the flexibility method or energy principles
v. Creating equilibrium equations in terms of the idealized element for each set of nodes of the discretized continuum
vi. Resolve the nodal displacement equilibrium.
vii. Evaluate the support reactions occurring at the constrained nodes in the event of displacement.

viii. The measurement of strains and stresses at various places within the elements.

FEM is generally guided by the principle that says that depending on the input and output parameters, applying boundary conditions (such as force, density, displacement) beyond the capability of a given body can lead to numerous circumstances with various configurations. It is well known that the heat produced by the arc on the workpiece surface and the transfer of heat energy into the workpiece are both necessary for successful TIG welding operations. An arc is created when the electrode is pointed toward the workpiece (leaving a small air gap), and this arc is utilized to melt and fuse the workpiece at a high temperature [14].

Using SOLIDWORKS 2021 version, 10-mm CAD model of the mild steel plate examined in this study was modelled in accordance with the dimensions presented in Fig. 3. With SOLIDWORKS Premium, the simulation was run. The simulation was performed using the Thermal simulation programme. With the findings of the initial study serving as a sensor, a design study was conducted. The results of a total of 15 runs, including responses for thermal conductivity and weld dilution, are given. Eight bodies make up the model. The parent metal is represented by two bodies, and the shape of the weld bead is represented by the other smaller bodies. As seen here, the original metal was a $60 \times 40 \times 10$ mm plate. Summary of model information is presented in Table 3.

Due to the specimen's temperature-dependent characteristics, the standard AISI 1020 was amended. The study properties for the thermal analysis are shown in Table 4.

After that, the model was subjected to a number of starting circumstances before a welding experiment was conducted on a sheet of 10-mm mild steel. At the start of the FEM welding experiment, the following circumstances were established:

i. The beginning temperature was set at 600 °C, providing an initial temperature gradient of 30 °C.
ii. About 60 W/m$^2$. K convection coefficient
iii. About 25 °C for the bulk ambient temperature

On the heat source, a trapezoidal time-dependent heat function was used. At several runs, the input heat power was altered. Voltage, current, and gas flow rate all influence the heat power. Equation 1 gives the heat power:

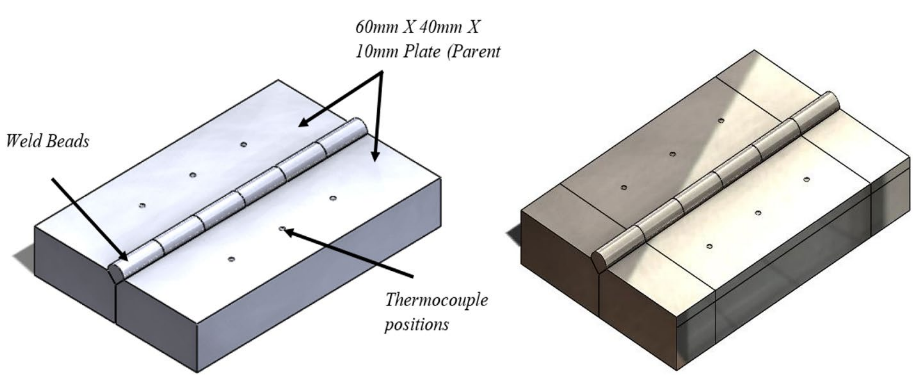


**Fig. 3** SOLIDWORKS geometric model

**Table 3** Summary of model information

| Name and Reference of Document | Resolv-ed as | Volumetric Characteristics | Path/Date(Document) |
|---|---|---|---|
| **Split Line2** 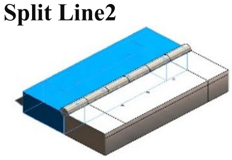 | Solid Body | Mass:0.0938483 kg<br>Volume:1.18795e-05 $m^3$<br>Density:7900 kg/$m^3$<br>Weight:0.919713 N | C:\Users\NW Green Solutions\Documents\Welding model\Base Metal.SLDPRT<br>Aug 28 05:46:32 2022 |
| **Split Line2** 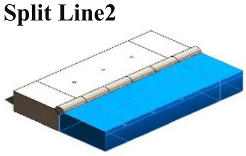 | Solid Body | Mass:0.0938483 kg<br>Volume:1.18795e-05 $m^3$<br>Density:7900 kg/$m^3$<br>Weight:0.919713 N | C:\Users\NW Green Solutions\Documents\Welding model\Base Metal.SLDPRT<br>Aug 28 05:46:32 2022 |
| **Boss-Extrude2** 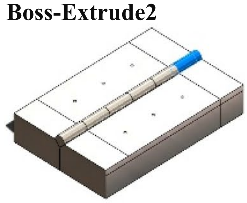 | Solid Body | Mass:0.000812372 kg<br>Volume:1.02832e-07 $m^3$<br>Density:7900 kg/$m^3$<br>Weight:0.00796124 N | C:\Users\NW Green Solutions\Documents\Welding model\Weld bead.SLDPRT<br>Aug 28 05:46:32 2022 |
| **Boss-Extrude2** 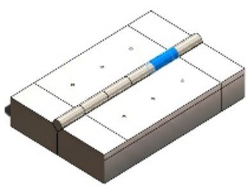 | Solid Body | Mass:0.000812372 kg<br>Volume:1.02832e-07 $m^3$<br>Density:7900 kg/$m^3$<br>Weight:0.00796124 N | C:\Users\NW Green Solutions\Documents\Welding model\Weld bead.SLDPRT<br>Aug 28 05:46:32 2022 |
| **Boss-Extrude2** 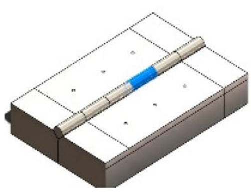 | Solid Body | Mass:0.000812372 kg<br>Volume:1.02832e-07 $m^3$<br>Density:7900 kg/$m^3$<br>Weight:0.00796124 N | C:\Users\NW Green Solutions\Documents\Welding model\Weld bead.SLDPRT<br>Aug 28 05:46:32 2022 |
| **Boss-Extrude2** 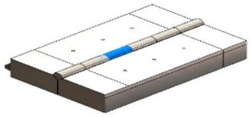 | Solid Body | Mass:0.000812372 kg<br>Volume:1.02832e-07 $m^3$<br>Density:7900 kg/$m^3$<br>Weight:0.00796124 N | C:\Users\NW Green Solutions\Documents\Welding model\Weld bead.SLDPRT<br>Aug 28 05:46:32 2022 |
| **Boss-Extrude2** 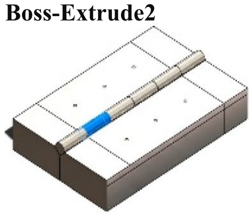 | Solid Body | Mass:0.000812372 kg<br>Volume:1.02832e-07 $m^3$<br>Density:7900 kg/$m^3$<br>Weight:0.00796124 N | C:\Users\NW Green Solutions\Documents\Welding model\Weld bead.SLDPRT<br>Aug 28 05:46:32 2022 |
| **Boss-Extrude2** 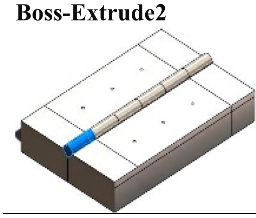 | Solid Body | Mass:0.000812372 kg<br>Volume:1.02832e-07 $m^3$<br>Density:7900 kg/$m^3$<br>Weight:0.00796124 N | C:\Users\NW Green Solutions\Documents\Welding model\Weld bead.SLDPRT<br>Aug 28 05:46:32 2022 |

**Table 4** Study of the properties of thermal analysis

| Study name | Welding parameters |
|---|---|
| Analysis type | Thermal (transient) |
| Mesh type | Solid mesh |
| Solver type | FFEPlus |
| Solution type | Transient |
| Total time | 20 s |
| Time increment | 2.5 s |
| Contact resistance defined | No |

$$P = nVI \tag{1}$$

where $V$ is the arc voltage, $I$ is the welding current, and $n$ is scaled as a factor by the gas flow rate to reflect the arc efficiency. Using the input variables obtained from the design experiment (centre composite design method), the simulation was run 20 times.

#### Analysis type

The test run sheet, as depicted above, lists the voltage, current, gas flow rate, and accompanying weld dilution and thermal conductivity findings for each run to create an environment that is thermally stable. Implemented was a transient thermal analysis with 100 steps and a 0.1-s step time. In order to prevent heat transmission from the weld beads to the plates at starting time zero, a temperature of 298 K was applied to the plate and weld beads.

#### Environmental conditions

The environmental factors revealed that at air velocities less than 4 m/s$^2$, the average convection coefficient of air over a metal surface is 25 W/m$^2$ K. According to experiments, the average ambient temperature is 24.5 °C. All exposed faces in SOLIDWORKS have the convection option turned on, with the exception of the bottom face. Convection across the weld bead shape was thought to have little impact on the thermal data. For all bodies, including weld beads, an initial temperature of 25 °C was applied at the body level. The model environmental thermal loads are shown in Table 5.

#### Material properties

For the sake of simplicity, AISI 1020 was considered to be the standard for all parent and filler materials. To meet the demands of this research, the steel's thermal characteristics have been altered. The properties that were given to the model in SOLIDWORKS 2018 are as follows. Table 6 lists the reference model's material characteristics. Ten-millimetre (10 mm) plate was obtained from Universal Steel Rolling Mill, Ogba-Ikeja, Lagos, Nigeria, and analysis for mechanical properties and chemical composition, which revealed that the material is AISI 1020 low carbon steel was determined in the same company using the mass spectrometer. The mechanical properties and composition of AISI 1018 mild steel plate are presented in Table 6.

**Table 5** Table showing environment thermal loads

| Load name | Load image | Load details | |
|---|---|---|---|
| Initial temperature | 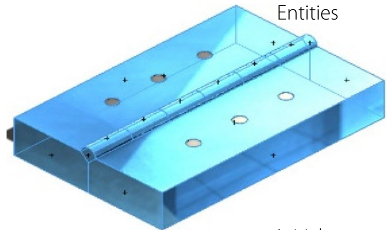 | Entities | 16 face(s) |
| | | Initial temperature | 298 Kelvin |
| Convection | 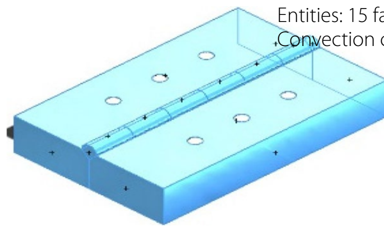 | Entities: 15 face(s)<br>Convection coefficient: 25 W/($m^2$.K) | |

**Table 6** Properties and composition of AISI 1020 mild steel plate

| S/no | Metal elements | percentage | Properties | Values |
|---|---|---|---|---|
| 1 | C | 0.094 ± 0.043 | Yield strength | 351.571 N/$mm^2$ |
| 2 | Si | 0.210 ± 0.043 | Tensile strength | 420.507 N/$mm^2$ |
| 3 | Mn | 0.310 ± 0.73 | Elastic modulus | 200,000 N/$mm^2$ |
| 4 | P | 0.056 ± 0.40 | Poisson's ratio | 0.29 |
| 5 | Cu | 0.094 ± 0.109 | Mass density | 7900 g/$cm^3$ |
| 6 | Al | 0.002 ± 0.004 | Shear modulus | 77,000 N/$mm^2$ |
| 7 | S | 0.022 ± 0.114 | Thermal expansion coefficient | 1.5e-005 K |
| 8 | Cr | 0.214 ± 0.073 | Yield strength | 351.571 N/$mm^2$ |
| 9 | Ni | 0.315 ± 0.120 | Tensile strength | 420.507 N/$mm^2$ |
| 10 | Fe | 98.32 ± 52 | Specific heat | 420 J/(kg.K) |

### Mesh details

In order to establish several important characteristics, including element shape, midside node placement, and element size, mesh control was applied to the heat source. Since the ellipsoidal shape of the heat source makes it more likely for stress to build in areas of higher curvature, a curvature-based mesh was also used to refine all of these areas. These details mostly pertain to the model-development process and may have an impact on the model's correctness and subsequent analysis. The meshed model is displayed in Fig. 4, and the mesh details are reported in Table 7.

### FEM optimization of weld dilution

The temperature charts show that the thermal distribution per weld bead section is comparable; the heat zone was thought to be completely circular. Cut plots were utilized to probe the edges on the plate's horizontal and vertical edges close to the

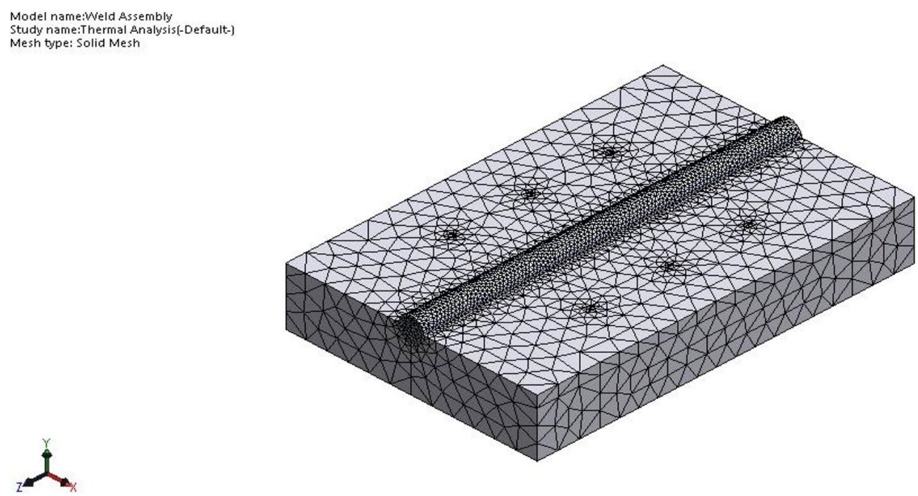


**Fig. 4** Meshed model using SOLIDWORKS mesher

**Table 7** Mesh details for the FEM model

| Mesh properties | Mesh details |
|---|---|
| Mesh type | Solid mesh |
| Mesher used | Blended curvature-based mesh |
| Jacobian points | 4 points |
| Maximum element size | 3.19061 mm |
| Minimum element size | 0.588517 mm |
| Mesh quality | High |
| Remesh failed parts with incompatible mesh | Off |
| Total nodes | 49,100 |
| Total elements | 32,388 |
| Maximum aspect ratio | 10.105 |
| % of elements with aspect ratio < 3 | 97.7 |
| % of elements with aspect ratio > 10 | 0.0124 |
| % of distorted elements (Jacobian) | 0 |
| Time to complete mesh (hh; mm; ss) | 00:00:03 |

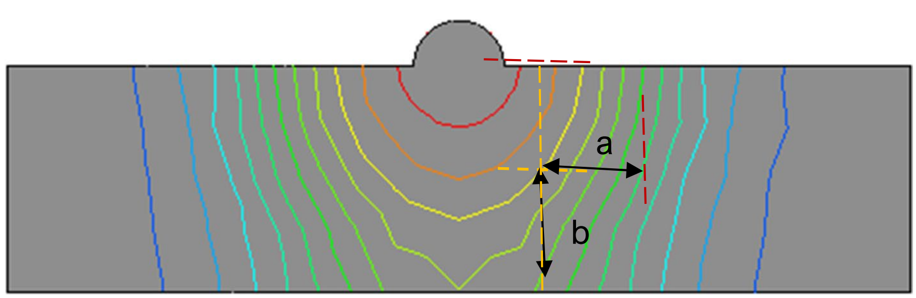


**Fig. 5** Fusion zone's distance along its horizontal and vertical axes

groove in order to confirm this supposition. As demonstrated in Fig. 5, the weld dilution is determined by looking at the distance on both the horizontal and vertical axes.

The parent and filler metals were melted together and mixed in the weld pool during the welding process. Dilution rate was a result of the parent metal and filler wire being mixed together after fusion to form the weld deposit, which caused a change in the metal chemistry of the weld. In addition, a piece of the parent metal was also melted by the molten electrode metal. The results of this were as follows:

i. The molten weld metal was diluted to create a weld bead chemistry that is made up of the parent metal diluted with the deposited metal (typically 10 to 30%).
ii. The weld pool's" surrounding material that is removed from above the upper.

## Results and discussion

The welding parameters, which in this case included welding current, voltage, and gas flow rate, were seen to influence the rate or percentage of weld dilation after each weld run in one way or another, as shown in Table 8. Combining the aforementioned welding settings on each weld cycle resulted in the welding temperatures, heat rates, melting rates, and percentage of weld dilution shown in Table 8. Despite not being determined experimentally, the welding heat rate and the metals' melting rates were compiled and extracted from FEM calculations pertaining to each of the weld runs.

**Table 8** Percentage of weld dilution obtained through experiments and FEM approach

| Weld runs | Current | Voltage | Gas flow rate | Max welding temperature | Heat rate | Melting rate | FEM % dilution | Ex percentage dilution |
|---|---|---|---|---|---|---|---|---|
| 1 | 240 | 20.98 | 13.5 | 3419 | 51.6 | 40.6 | 60.1 | 59.03 |
| 2 | 210 | 22 | 16 | 3415 | 49.7 | 39.4 | 58.2 | 57.0 |
| 3 | 250.23 | 23.5 | 13.5 | 3688 | 66.4 | 52.6 | 73.1 | 71.55 |
| 4 | 210 | 25 | 16 | 3411 | 47.2 | 37.2 | 56 | 55.02 |
| 5 | 250.23 | 20.98 | 13.5 | 3458 | 63.5 | 49.5 | 70.8 | 68.7 |
| 6 | 210 | 20.98 | 14.5 | 3407 | 45.3 | 35.7 | 54.6 | 53.22 |
| 7 | 225 | 24.5 | 11.98 | 3438 | 58.3 | 47.2 | 67.3 | 66.54 |
| 8 | 210 | 22 | 16 | 3425 | 54.1 | 43.5 | 63.2 | 61.03 |
| 9 | 225 | 26 | 14.5 | 3461 | 64.1 | 50.3 | 71.6 | 68.94 |
| 10 | 225 | 25 | 16 | 3427 | 55.7 | 44.3 | 64.7 | 63.12 |
| 11 | 199.77 | 23.5 | 14.5 | 3427 | 55.2 | 44.6 | 64.7 | 63.04 |
| 12 | 210 | 22 | 16 | 3409 | 48.4 | 36.3 | 55.2 | 54.23 |
| 13 | 250.23 | 24.5 | 14.5 | 3458 | 63.1 | 49.0 | 70.1 | 69.02 |
| 14 | 199.77 | 26 | 11.98 | 3397 | 40.4 | 29 | 49.8 | 47.2 |
| 15 | 250.23 | 22 | 11.98 | 3462 | 65.3 | 51.4 | 72.4 | 70.46 |
| 16 | 225 | 22 | 13.5 | 3401 | 42.7 | 32.4 | 51.7 | 48.36 |
| 17 | 199.77 | 26 | 11.98 | 3390 | 37.2 | 26 | 46.8 | 44.5 |
| 18 | 240 | 25 | 16 | 3442 | 59.6 | 48.7 | 68.8 | 65.55 |
| 19 | 240 | 20.98 | 13 | 3430 | 56.2 | 48.3 | 65.7 | 63.94 |
| 20 | 199.77 | 24.5 | 13.5 | 3403 | 43.5 | 33.3 | 52.7 | 49.54 |

A comparison between the percentage of weld dilution predicted using FEM and weld dilution determined using an experimental technique is shown in Fig. 6. Twenty weld runs produced using both an experimental and FEM technique show correlation between the measured and anticipated weld dilution histories on the fusion zone of the parent metal. Figure 6's weld dilution curve, which can be seen for both the FEM and experimental approaches, provides evidence of this. For instance, maximum and minimum weld dilution values of 71.55 and 44.5% were measured using an experimental technique at the same weld runs, while maximum and minimum weld dilution values of 73.1 and 46.8% were computed with FEM for weld runs 3 and 17.

For arc welding procedures, heat input is a crucial element that needs to be carefully managed in order to produce reliable welds. It is a property that has to do with how much electrical energy is provided to a weld during the welding process or how much arc energy. Due to the admixture of the base metal or the previously deposited weld metal, it has an impact on a welded material by changing the chemical composition of the weld metal.

A plot of experimental and FEM weld dilution at various heat inputs is shown in Fig. 7. The plot shows that maximum and minimum weld dilution values of 71.55 and 44.5% were measured experimentally at the same rate of arc heat input, while maximum and minimum weld dilution values of 73.1 and 46.8% were computed with FEM at arc heat input of 66.4 and 37.2 J/mm.

A relationship between high heat input and a high percentage of weld dilution and vice versa can be inferred from the plot's curvature. The 20 weld runs produced for both the FEM and experimental approaches show correlation between the measured and anticipated weld dilution at every step of fusion that requires heat input. This is demonstrated in Fig. 7.

Despite the fact that the microstructural properties were not taken into account in this study, it is important to note that heat input has a significant impact on the rate at which welds cool because it can change the microstructure of the weld metal and the heat-affected zone (HAZ) during or after welding [15–18]. For instance, since they produce embrittlement in the heat-affected zone, quicker cooling rates may be bad for a weldment. The mechanical characteristics of weld metal and the heat-affected zone (HAZ)

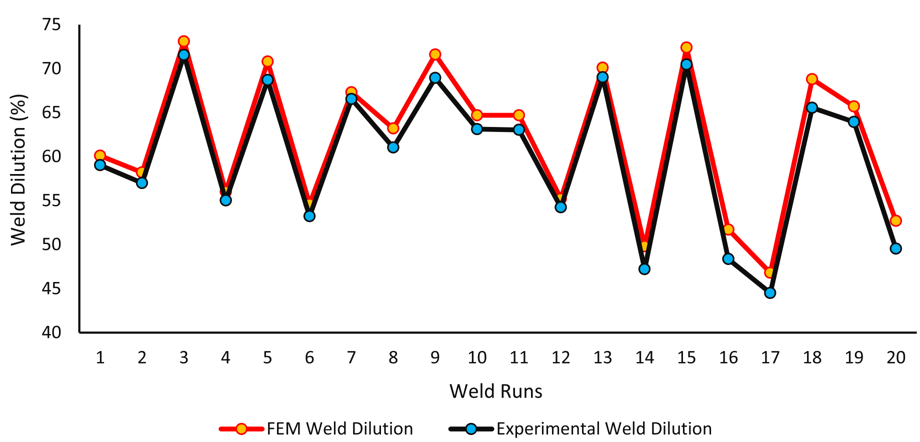


**Fig. 6** Plot of experimental and FEM weld dilution at different weld runs

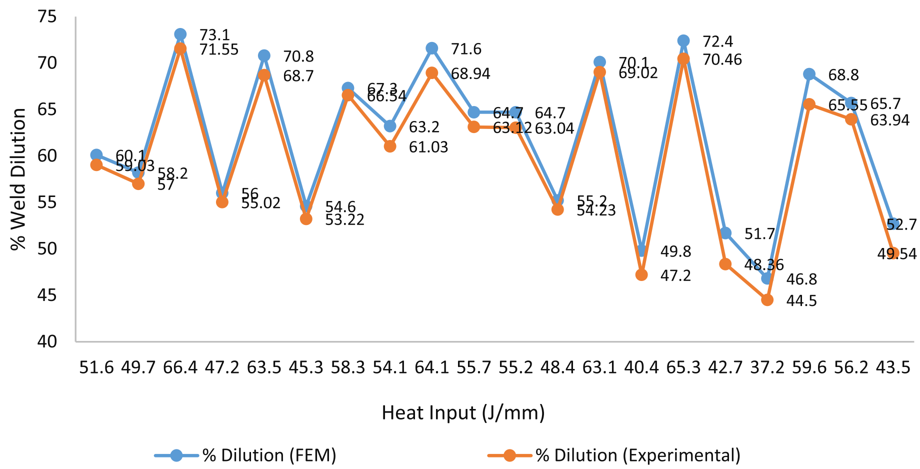


**Fig. 7** Plot of experimental and FEM weld dilution at different heat inputs

are directly impacted by changes in microstructure [19–21]. Therefore, it is crucial to manage the heat input in order to produce a solid microstructure and a weld of high quality.

The heat transfer during the entire cycle from arc heating to solidification and cooling to room temperature is a crucial factor in the welding process. The complex phenomena of heat flow around the fusion zone depends on a number of variables, such as temperature and welding amperage. According to studies conducted by Ikpe et al. [22] and Hasan et al. [23], a larger welding current causes a higher welding temperature, which increases the melting rate of the welded metal. High temperatures can have the effect of accelerating the melting rate of metals subjected to welding processes. The melting rate, which is a function of welding temperature, may have a significant impact on the percentage of weld dilution. By changing the chemical makeup of the weld, this in turn affects the proportion of weld dilution.

Figure 8, which depicts the plot of experimental and FEM weld dilution at various melting rates, demonstrates this. From the plot, it can be seen that maximum and minimum weld dilution values of 71.55 and 44.5% were measured experimentally at the same melting rate, while maximum and minimum weld dilution values of 73.1 and 46.8% were estimated with FEM at melting rates of 52.6 and 26 g/m. The plot's curvature reveals a relationship between the melting rate of the metal during welding and a high percentage of weld dilution and vice versa.

The 20 weld runs produced for both the FEM and experimental approaches in this work show correlation between the measured and anticipated weld dilution at every step of fusion that involves heat input, heat transfer, and melting rate. Heterogeneous fillings are invariably diluted by the base metal because fusion welding necessitates or demands that a portion of each base metal or substrate involved in the junction melt along with the filler. Dilution varies according to the following:

i. The joint type and joint edge preparation
ii. The welding procedure, its variables (such as the operating current mode), and the technique employed

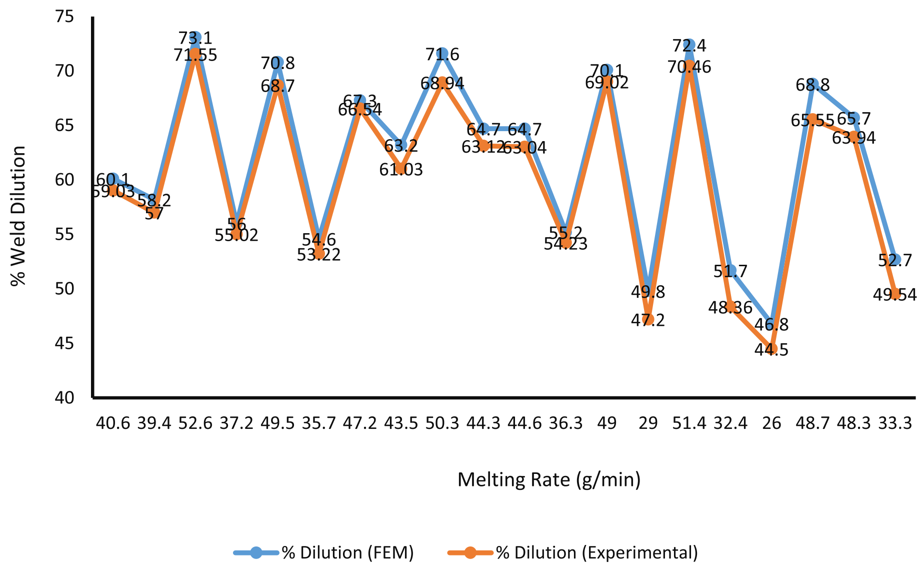


**Fig. 8** Plot of experimental and FEM weld dilution at different melting rates

iii. The incompatibility of the base metal and filler and, typically, the proportion of dilution (D)

The welded metals undergo arc heating throughout a temperature range for efficient fusion during the TIG welding process and are then allowed to cool. In this instance, the arc heating or welding temperature of the fused metals started when the material's temperature was 28 °C, and it increased significantly until it reached its peak temperature of roughly 36 °C when fusion was effectively established.

The metal being welded underwent metallurgical and mechanical modifications as a result of the heating and cooling process. Other welding factors, such as weld dilution, heat rate, melting rate, and so on, are also impacted by these changes. Here, the high welding temperature generates a lot of heat around the fusion zone. This is the heat input that is applied evenly throughout the welded area, and when it reaches or approaches the metal's melting point, it induces melting everywhere around the fusion zone. At this point, fusion has already begun to take place, and the melting rate is at its highest, allowing for successful fusion.

These stages complete the thermal cycle of the welded material, during which phase transformation takes place and the chemical composition of the welding filler material is changed as a result of the base material's admixture with the deposited weld bead or previously deposited weld metal, and this results in weld dilution. The plot of experimental and FEM weld dilution at various welding temperatures, heating rates, and melting rates is shown in Fig. 9. The plot shows that maximum and minimum weld dilution values of 71.55 and 44.5% were measured experimentally at the same welding temperatures, whereas maximum and minimum values of 73.1 and 46.8% were computed with FEM at maximum welding temperatures of 3688 and 3390 °C.

The weld dilution curves' trend showed a connection between the experimental and FEM approaches. Additionally, at maximum welding temperatures of 3688 and

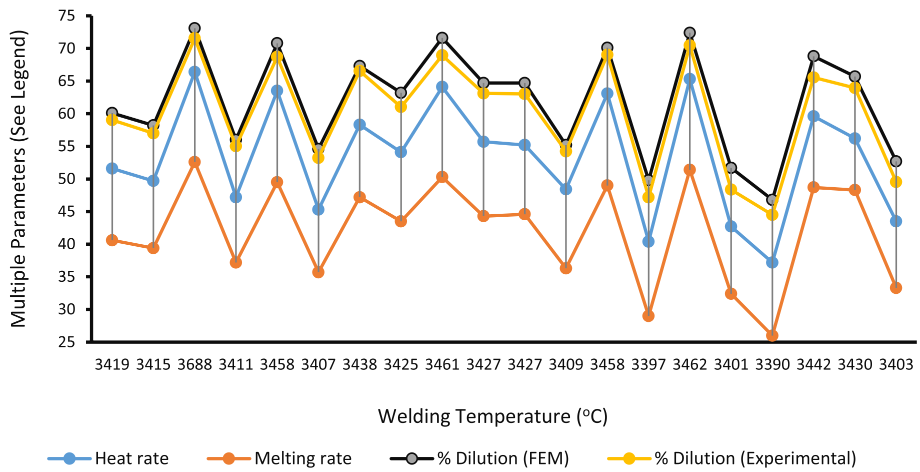


**Fig. 9** Plot of experimental and FEM weld dilution at multiple weld parameters

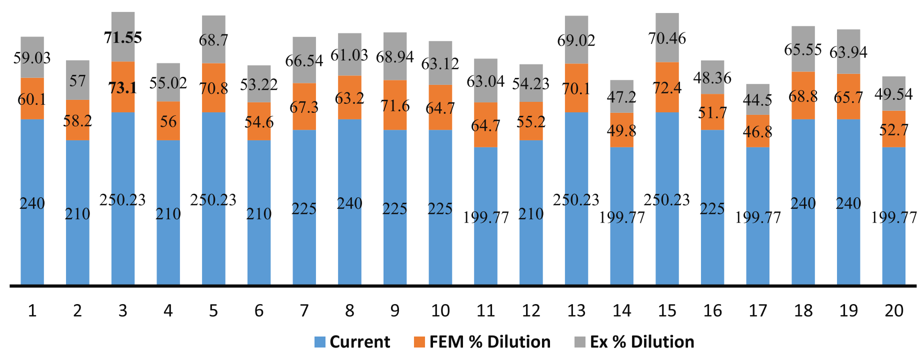


**Fig. 10** Plot of experimental and FEM weld dilution at different welding currents

3390 °C, maximum and lowest heating and melting rates of 66.4 and 37.2 J/mm and 52.6 and 26 g/min, respectively, were estimated using FEM. Figure 9 shows that, in both directions, a rise in welding temperature increased weld dilution percentage, heat distribution rate, and melting rate.

A welding parameter called welding current describes the flow of electricity through the arc gap between the electrode's tip and the metal being welded. The movement of electrons (electricity) is known as an electric current. Heat is produced when there is a resistance to the passage of electrons, which go from negative (−) to positive (+). The amount of heat and temperature that the arc produces increases with electrical resistance, which has some effects on the pace of weld dilution. For instance, low weld corrosion resistance may result from significant weld dilution, which is a result of high welding temperature gradient on the welded metal.

This is so because a weld with a high carbon concentration is more prone to corrosion due to high dilution. In other words, increase in dilution enhances the carbon content and reduces the chromium content of the claddings resulting in high DOS [24, 25]. High dilution can also result in a decline in the weld's mechanical qualities, including its hardness and strength. The link between welding current and weld dilution as determined by FEM and experimental procedure is shown in Fig. 10. According to the plot, maximum and minimum weld dilution were calculated using FEM at the same maximum and minimum welding currents as maximum and minimum weld dilution obtained from the experimental process were 71.55 and 44.5% and 73.1 and 46.8%, respectively.

This correlates to the findings of Ohwoekevwo et al. [26] in a similar study, where the maximum and minimum wilding currents and weld dilution fell in the same range obtained in this paper. The FE results were validated with the experimental results. A significant correlation was observed in each of the 20 weld runs obtained from experimental and FEM weld dilution output response.

Weld dilution and welding current are plotted in Fig. 10, and it can be seen that as welding current increased, weld dilution % also increased and vice versa. This correlates with the findings of Ohwoekevwo et al. [27] who also stated in a study on prediction of percentage dilution in AISI 1020 low carbon steel welds produced from tungsten inert gas welding that percentage of weld dilution for artificial neural network (ANN), and experimental results at each weld run increased as the welding current also increased and vice versa.

Figure 11a–f depicts sectional views of the weld dilution profile. The simulation of the 1-mm low carbon steel plate model using the finite element method produced these profiles. It can be seen that red colours appear at the top of the colour band on the simulated models, while royal blue colours appear at the bottom. Red, royal blue, and all other colours on the colour band have percentages of weld dilution values linked to them. The proportion of maximum weld dilution caused by the highest welding temperature is indicated by weld dilution values in red, while those in royal blue are indicated by weld dilution values.

The parent material next to the weld was heated up during the welding operation. The material's temperature is promptly raised to a level that is just below but close to its melting point and then rapidly cooled. The melting process is due to heat conduction and convection, resulting in weld dilution across the weld pole. Weld dilution is the change in chemical composition of the weld metal as a result of the base metal component that melts and begins to form the fusion zone [28]. The mass, specific heat, beginning temperature, and heat input of the welding process all affect how quickly the parent material cools.

The fusion zone, which is a section of the welded low carbon steel plate that has undergone melting, and the heat-affected zone (HAZ), which is a section of the material that is partially melted by the welding heat, are the features that define the weld dilution profiles. The following zones can be found within the HAZ in steels, according to the highest welding temperature that the arc welding process achieves: grain growth zone is that portion of the heat-affected zone (HAZ) that is heated beyond the temperature necessary for grain growth and extends up to the fusion border zone, beyond 1150 °C to peritectic

(See figure on next page.)

**Fig. 11** **a** Sectional view of weld dilution after 1 s at the maximum welding temperature (3430 °C). **b** Sectional view of weld dilution after 2.5 s at the maximum welding temperature (3442 °C). **c** Sectional view of weld dilution after 4 s at the maximum welding temperature (3458 °C). **d** Sectional view of weld dilution after 5.5 s at the maximum welding temperature (3461 °C). **e** Sectional view of weld dilution after 7 s at the maximum welding temperature (3462 °C). **f** Sectional view of weld dilution after 8.5 s at the maximum welding temperature (3688 °C)

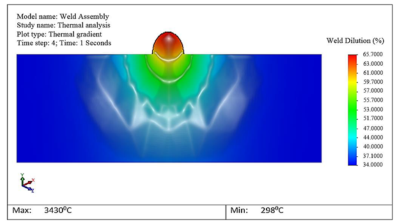


**Fig. 11a** Sectional view of weld dilution after 1 second at the maximum welding temperature (3430°C)

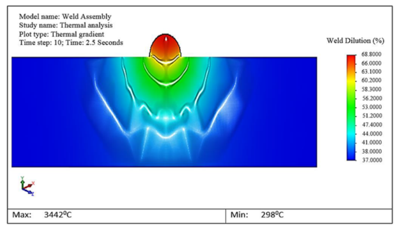


**Fig. 11b** Sectional view of weld dilution after 2.5s at the maximum welding temperature (3442°C).

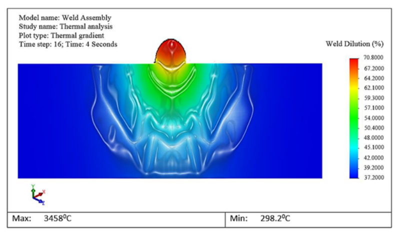


**Fig. 11c** Sectional view of weld dilution after 4s at the maximum welding temperature (3458 °C)

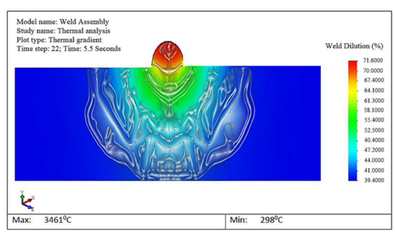


**Fig 11d** Sectional view of weld dilution after 5.5s at the maximum welding temperature (3461 °C)

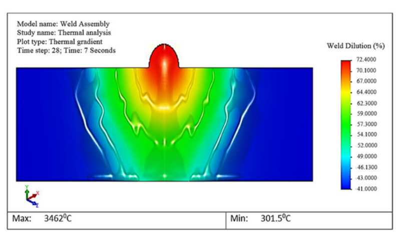


**Fig. 11e** Sectional view of weld dilution after 7s at the maximum welding temperature (3462 °C)

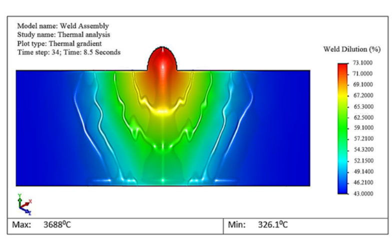


**Fig. 11f** Sectional view of weld dilution after 8.5s at the maximum welding temperature (3688 °C)

**Fig. 11** (See legend on previous page.)

temperature. Grain Refined Zone, 950 to 1150 °C, i.e., beyond A3 up to the grain refined temperature range, Partially Transformed Zone, 750 to 950 °C, or below A3 [29, 30].

Weld dilution is a phenomenon brought on by the heat of welding. This is a change in the weld metal brought on by mixing the weld metal or the weld metal that had already been deposited. In other words, due to absorption in the parent metal, the alloy composition of the weld metal decreases or undergoes dilution when two pieces of metal are joined by welding. The following factors influence the amount of weld dilution:

i. Joint edge preparation and the type of weld joint
ii. The welding procedure, the characteristics of the procedure, and the techniques used
iii. Incompatibility between the base metal and the filler

However, improper welding process control might lead to several welding flaws that could ultimately result in the failure of the weld joint. Weld porosity, lack of fusion, inadequate penetration, weld undercut, etc. are some typical weld problems linked to improperly regulated weld dilution. Sectional views of weld dilution simulation profiles at different seconds (1, 2.5, 4.5, 5.5, 7, and 8.5 s) at maximum welding temperatures (3430, 3442, 3458, 3461, 3462, and 3688 °C) are shown in Fig. 11a–f respectively.

This agrees with the findings obtained by Ohwoekevwo et al. [26] which revealed that increase in welding time steps of 1, 2.5, 4, 5.5, 7, and 8.5 s corresponded with increase in welding temperature with maximum values of 3430, 3442, 3458, 3461, 3462, and 3688 °C. The aforementioned welding temperature effect led some variations with maximum weld dilution in the order of 65.70, 68.80, 70.80, 71.60, 72.40, and 73.10%, respectively. A significant correlation was observed in each of the 20 weld runs obtained from experimental and FEM weld dilution output response.

The welding input parameters in Table 8 are responsible for the maximum welding temperature and weld dilution obtained in this paper. It is observed that welding input parameters of 250.23 A current, 23.5 V voltage, and 13.5 m/L gas flow rate produced maximum welding temperature of 3688 °C which lead to maximum FEM predicted weld dilution of 73.1% and experimentally determined maximum weld dilution of 71.55%. Similarly, welding input parameters of 199.77 A current, 26 V voltage, and 11.98 m/L gas flow rate produced maximum temperature of 3390 °C which lead to minimum FEM predicted weld dilution of 46.8% and experimentally determined minimum weld dilution of 44.5%. Dinesh and Sunil [31] reported weld dilution of 47.61%, Kumari et al. [32] reported weld dilution of 46.05%, while Kingsley-omoyibo [33] reported weld dilution of 45.73% for TIG welding operation. Studies have shown that lower weld dilution which is obtained from lower welding temperature is ideal for steel materials [34–36]. Therefore, it is important to adequately control welding input parameters in order to obtain quality welds.

## Conclusions

Thermal investigation of AISI 1020 low carbon steel plate that has undergone an experimental gas tungsten arc welding technique was done in this work. Later, the dynamics of the welded material were studied using a finite element computational approach. The following conclusions from the study were arrived at during the course of the study.

i. It is discovered that a high heat input and a high percentage of weld dilution are related. To put it another way, increasing the heat input will result in more thermal energy and, thus, more dilution.
ii. It has been found that a high percentage of weld dilution and a high melting rate of the metal when welding are related.
iii. Weld dilution and welding current were plotted, and it was discovered that an increase in welding current also caused an increase in the percentage of weld dilution and vice versa.
iv. In this instance, the heat flux and welding temperature increased and dropped in pari passu, showing that the opposite is true in that the greater the welding temperature, the higher the heat flux.
v. The weld profiles clearly showed that the fusion zone was where the welding heat input and temperature reached their greatest levels. Beyond this zone, the heat transfer decreases as it passes through the HAZs. This is as a result of the welding heat traveling from a region of higher temperature (fusion zone) to the region of lower temperature (grain growth zone, recrystallized zone, partially transformed zone, tempered zone, and unaffected base metal). The size of HAZ is influenced by the level of thermal diffusivity, which is dependent on the thermal conductivity, density, and specific heat of a substance as well as the amount of heat going in to the material.

Therefore, the welding process should be carefully monitored while also choosing the best welding input variable to reduce the likelihood of weld flaws that could ultimately result in the failure of the weld joint.

**Abbreviations**

| | |
|---|---|
| AISI | American Iron and Steel Institute |
| FEM | Finite element method |
| TIG | Tungsten inert gas |
| GTAW | Gas tungsten arc welding |
| HAZ | Heat-affected zone |
| SA | Submerged arc |
| RSM | Response surface methodology |
| GMAW | Gas metal arc welding |
| NPD | Nozzle-to-plate distance |
| WFR | Wire feed rate |
| GMAW | Gas metal arc welding |
| GTA | Gas tungsten arc |
| SEM | Scanning electron microscopy |
| EDS | Energy-dispersive spectroscopy |
| CCD | Central composite design matrix |
| FEA | Finite element analysis |
| CAD | Computer-aided design |
| s | Seconds |
| K | Kelvin |
| ANN | Artificial neural network |
| °C | Degrees Celsius |

**Acknowledgements**
The authors have benefited greatly from the discussions about this topic with Engr. Victor our PhD supervisor (who encouraged us in developing this research study). We would like to thank our families and friends for their love and support throughout the research process.

**Authors' contributions**
MB, conceptualization, development, modeling, simulation, experimentations, and analysis. JO, investigation and delivered resources. AI, supervision, guidelines, investigation, and delivered resources. All authors have read and approved the manuscript.

**Funding**
The authors received no funding for the research study.

**Availability of data and materials**
Data can be shared upon request even if it is mentioned that the data is in the article.

## Declarations

**Competing interests**
The authors declare that they have no competing interests.

Received: 13 June 2023 Accepted: 21 January 2024
Published online: 06 February 2024

**References**

1. Owunna IB, Ikpe AE, Achebo JI (2018) Temperature and time dependent analysis of tungsten inert gas welding of low carbon steel plate using Goldak model heat source. J Appl Sci Env Mgt 22(11):1719–1725
2. Owunna I, Ikpe AE (2019) Finite element analysis of tungsten inert gas welding temperatures on the stress profiles of AISI 1020 low carbon steel plate. Int J Eng Tech 5(2):50–58
3. Sun YL, Hamelin CJ, Smith MC, Vasileiou AN, Flint TF, Francis JA (2018) Modelling of dilution effects on microstructure and residual stress in a multi-pass weldment. ASME 2018 Pressure Vessels and Piping Conference, Prague, Czech Republic, pp 1–12
4. DuPont JN, Marder AR (1996) Dilution in single pass arc welds. Metall Mater Trans B27:481–489
5. Francis JA, Bednarz B, Bee J (2002) Prediction of steady state dilution in multipass hardfacing overlays deposited by self-shielded flux cored arc welding. Sci Tech Weld Join 7:95–101
6. Hunt A, Kluken A, Edwards G (1994) Heat input and dilution effects in micro alloyed steel weld metals. Weld J 73:9s–15s
7. Sehrawat A (2020) Development of mathematical model to predict weld dilution for GMA welding of stainless steel 301. Int J Res App Sci Eng Tech 8(8):57–65
8. Lu L, Cai Z, Yang J, Liang Z, Sun Q, Pan J (2022) Study on key parameters of dilution ratio of the bead deposited by GTAW method for nuclear components. Metals 12(1506):1–17
9. Aghakhani M, Jalilian MM, Karami A (2012) Prediction of weld bead dilution in GMAW process using fuzzy logic. App Mech Mat 110–116:3171–3175
10. Sun YL, Obasib G, Hamelinc CJ, Vasileioua AN, Flinta TF, Balakrishnana J, Smitha MC, Francisa JA (2019) Effects of dilution on alloy content and microstructure in multi-pass steel welds. J of Mat Pro Tech 265:71–86
11. Sun YL, Hamelin CJ, Vasileiou AN, Xiong Q, Flint TF, Obasi G, Francis JA, Smith MC (2020) Effects of dilution on the hardness and residual stresses in multipass steel weldments. Int J Pres Ves P. 187(104154):1–13
12. Zhang Z, Huang X, Yao P, Xue J (2021) A new method for weld dilution calculation through chemical composition analysis. Metals 11(1):131
13. Owunna IB, Ikpe AE (2022) Hardness characteristics of AISI 1020 low carbon steel weldment produced by tungsten inert gas welding. Nig J Eng 29(1):36–42
14. Ikpe AE, Itiat NE, Bassey MO (2023) Time-variant analysis on experimental and computational TIG welding temperature transition across fusion and heat affected zones of AISI 1018 mild steel plate. Tokyo 7th International Innovative Studies and Contemporary Scientific Research Congress, Tokyo, Japan, pp 270–290
15. Higelin A, Le Manchet S, Passot G, Cissé S (2022) Heat-affected zone ferrite content control of a duplex stainless steel grade to enhance weldability. Weld World 66:1503–1519
16. Bharadwaj V, Rai AK, Upadhyaya BN, Singh R, Rai SK, Bindra KS (2022) A study on effect of heat input on mode of welding, microstructure and mechanical strength in pulsed laser welding of Zr-2.5 wt.%Nb alloy. J Nuclear Mater 564:153685
17. Owunna IB, Ikpe AE, Ohwoekevwo JU (2022) Application of SEM/EDS in fractographic investigation of TIG welded AISI 1020 fusion zones at distinct welding current steps. Arid Zone J Eng Technol Environ 18(2):255–266
18. Liu H, Lv S, Xuan Y, Oliveira JP, Schell N, Shen J, Deng J, Wang Y, Yang J (2023) Effects of heat input on weld microstructure and properties in keyhole TIG welding of Invar 36 alloy. Materials 16:3692
19. Stadler M, Schnitzer R, Gruber M, Steineder K, Hofer C (2021) Microstructure and local mechanical properties of the heat-affected zone of a resistance spot welded medium-Mn steel. Materials 14(12):3362
20. Han HG, Wang F, Lu YH, Han YM, Chen ZZ (2023) A study on as-welded microstructure and mechanical properties of thick-walled 9Cr3W3Co1CuVNbBN martensitic steel weldment. Int J Press Vessels Pip 206:105077
21. Senthilkumar S, Manivannan S, Venkatesh R, Karthikeyan M (2023) Influence of heat input on the mechanical characteristics, corrosion and microstructure of ASTM A36 steel welded by GTAW technique. Heliyon 9(9):1–12
22. Ikpe AE, Owunna IB, Ikpe E (2017) Effects of arc voltage and welding current on the arc length of tungsten inert gas welding (TIG). Int J Eng Tech 3(4):213–221
23. Hasan A, Ali OM, Alsaffawi AM (2018) Effect of welding current on weldments properties in mig and TIG welding. Int J Eng Tech 7(4.37):192–197
24. Nunes MM, Gomes JH, Brito TG, Renzetti RA (2020) Effect of flux cored arc welding process parameters on corrosion resistance of austenitic stainless steel claddings. Mater Res 23(6):1–8

25. Heider B, Oechsner M, Reisgen U, Ellermeier J, Engler T, Andersohn G, Sharma R, Olivares EG, Zokoll E (2020) Corrosion resistance and microstructure of welded duplex stainless steel surface layers on gray cast iron. J Therm Spray Technol 29:825–842
26. Ohwoekevwo JU, Achebo JI, Ikpe AE (2023) Finite element modelling and simulation of weld dilution rate from tungsten inert gas (TIG) welding experiment on AISI 1020 low carbon steel plate. 10$^{th}$ Int Zeugma Conf Sci Res. 2023/ Gaziantep, Turkey
27. Ohwoekevwo JU, Ozigagun A, Achebo JI, Obahiagbon KO (2023) Prediction of percentage dilution in AISI 1020 low carbon steel welds produced from tungsten inert gas welding. J Appl Sci Env Mgt 27(5):979–984
28. Lin Z, Ya W, Subramanian VV, Goulas C, Castri B, Hermans MJ, Pathiraj B (2020) Deposition of Stellite 6 alloy on steel substrates using wire and arc additive manufacturing. The Int J Adv Manuf Tech 111:411–426
29. Sura N, Mittal V (2015) Experimental study on effects of process parameters on HAZ of plain carbon steel using GMAW. Int J Lat Res Sci Tech 4(2):167–170
30. Owunna I, Ikpe AE (2018) Effects of parametric variations on bead width of gas tungsten arc welding of AISI 1020 low carbon steel plate. Int J Eng Tech Sci 5(3):1–13
31. Dinesh K, Sunil P (2012) Dilution control by advanced SAW. Int J Adv Mater Res 488(489):1737–1741
32. Kumari P, Mohd S, Prarvez M (2013) Effect of MIG welding input process parameters on weld bead geometry on HSLA steel. Int J Eng Sci Technol 1(1):200–215
33. Kingsley-Omoyibo QA (2020) Optimization of percentage dilution in butt welds to prevent weld porosity using response surface methodology. Int J Innovative Res Dev 9(6):91–98
34. Nouri M, Abdollah-zadehy A, Malek F (2007) Effect of welding parameters on dilution and weld bead geometry in cladding. J Mater Sci Technol 23(6):817–822
35. Sun YL, Obasi G, Hamelin CJ, Vasileiou AN, Flint TF, Balakrishnan J, Smith MC, Francis JA (2029) Effects of dilution on alloy content and microstructure in multi-pass steel welds. J Mater Process Technol 265:71–86
36. Aggarwal S, Dwivedi M, Khanna P (2022) Mathematical modelling to predict the dilution in FCA welded low carbon steel plates. Mater Today Proceed 56(6):3512–3519

## Publisher's Note